Design of Aerogravity-Assist Trajectories

Wyatt R. Johnson* and James M. Longuski[†]
Purdue University, West Lafayette, Indiana 47907-1282

Aerogravity-assist trajectories are optimized in the sense of maximizing ΔV obtained by the flyby, maximizing aphelion, minimizing perihelion, and minimizing the time of flight for a particular destination planet. A graphical method based on Tisserand's criterion is introduced to identify potential aerogravity-assist trajectories. To demonstrate the application of the theory, patched-conic trajectories are computed to each planet in the solar system. For a lift-to-drag ratio of 7 and a launch excess velocity of 6.0 km/s, Pluto may be reached in 5.5 years using a Venus–Mars–Venus series of aerogravity assists.

Nomenclature

E	=	heliocentric specific orbital energy, km²/s²
g	=	gravitational acceleration at Earth's surface, 9.80665 m/s²
R	=	semimajor axis of aerogravity-assist (AGA) body, km
R_a	=	aphelion distance, km
R_p	=	perihelion distance, km
r_p	=	periapsis at AGA body, km
U	=	nondimensional heliocentric speed
U_∞	=	nondimensional excess velocity
V	=	heliocentric velocity of spacecraft, km/s
V_{pl}	=	velocity of planet with respect to sun, km/s
V_∞	=	excess velocity, km/s
α	=	angle between V_∞ and V_{pl}, rad
γ	=	flight-path angle, deg
ΔV	=	change of velocity magnitude, km/s
θ	=	aerodynamic turn angle, rad
μ	=	gravitational parameter, km³/s²
ϕ	=	total AGA turn angle, rad

Subscripts

pl	=	planet
1, 2	=	path indices
$\odot$	=	sun

Superscripts

−	=	preflyby
+	=	postflyby

Introduction

GRAVITY-ASSIST trajectories have become powerful aids in enabling humankind to explore the solar system. The Voyager II mission depended on gravity assists from multiple planets. The Galileo spacecraft used Earth and Venus to reach Jupiter; the Cassini spacecraft is using Earth, Venus, and Jupiter to reach Saturn. Plans for a mission to Pluto require up to four flyby bodies, with flight times ranging from 10 to 15 years[1] (compared to the Hohmann transfer time of 45 years). However, for a given planet and flyby V_∞, there is a limit to the bending (and thus the ΔV) that the gravity-assist technique can provide. Attempts to increase the spacecraft's heliocentric energy by employing more flybys often result in unacceptably long flight times to the destination body.

New technologies and new ideas may reduce the time of flight of gravity-assist trajectories. One approach is to replace the conic arcs between planets with faster low-thrust arcs.[2] Though this technique has merit, as the V_∞ at the flyby body increases, the ΔV gained becomes increasingly smaller (as in the case of the conventional gravity assist). Another idea involves flying a lifting body, for example, a waverider,[3] through the atmosphere of the flyby planet. Aerodynamic forces can augment the bending angle to arbitrarily large values. Lewis and McRonald[4] contend that the technology exists to build a waverider with lift-to-drag (L/D) ratios greater than 7. More recently, Starkey and Lewis[5,6] published results on high L/D waveriders, but optimized for flight regimes in terrestrial applications. The aerogravity-assist (AGA) maneuver could dramatically augment the gravity technique.[7,8] An AGA has the added advantage of yielding larger ΔV gains with higher flyby V_∞.

Because the turn angle in an AGA is arbitrary, an AGA can perform nearly as well in one flyby as several conventional gravity assists. There will be some energy losses due to drag, but this loss is more than made up for by the large heliocentric ΔV and the significant flight-time reduction. Preliminary work by McRonald and Randolph[8] and by Sims et al.[9] indicates that, with AGA, a spacecraft could reach Pluto in 5–7 years, with minimal launch energy. Bonfiglio[10] confirms the work of Sims et al.[9] by calculating several AGA trajectories to Pluto with the satellite tour design program (STOUR),[11] which Bonfiglio modified for the purpose. Finally, Lohar et al. compute optimal AGA atmospheric flythrough trajectories for a variety of cases.[12−14]

In this paper we find the maximum possible ΔV for an AGA maneuver and compute the performance envelope of AGA trajectories. We then apply a graphical technique to gain further insight into potential AGA trajectories and compute theoretical bounds on the minimum time of flight to each planet. Finally we propagate our predicted minimum time-of-flight (TOF) AGA paths in a patched-conic solver to find actual trajectories.

AGA Equations

A model relating pre- and postflyby V_∞ is given by[15]

$$V_\infty^+ = \left\{ \left(V_\infty^{-2} + \mu/r_p \right) \exp[-2\theta/(L/D)] - \mu/r_p \right\}^{\frac{1}{2}} \quad (1)$$

For convenience, we nondimensionalize this equation, using $U_\infty \equiv V_\infty^2/(\mu/r_p)$ to obtain

$$U_\infty^+ = \left(U_\infty^- + 1 \right) \exp[-2\theta/(L/D)] - 1 \quad (2)$$

We calculate the ΔV, and then the more convenient nondimensional ΔU from

$$\Delta V = V_\infty^{-2} + V_\infty^{+2} - 2V_\infty^- V_\infty^+ \cos\phi$$

$$\Delta U = U_\infty^- + U_\infty^+ - 2\sqrt{U_\infty^- U_\infty^+} \cos\phi \quad (3)$$

*Ph.D. Candidate, School of Aeronautics and Astronautics. Student Member AIAA.
†Professor, School of Aeronautics and Astronautics, 1282 Grissom Hall; longuski@ecn.purdue.edu. Associate Fellow AIAA.

Table 1 Percent error in approximating maximum AGA ΔU by different analytical approximations

	Elices[16]			Transcendental			Quadratic		
L/D	Maximum	Mean	MSE[a]	Maximum	Mean	MSE	Maximum	Mean	MSE
1	74	17	3.3	69	3.7	0.7	55	44	22
2	62	3.7	0.4	58	1.4	0.3	69	23	5.7
3	53	3.2	0.3	50	0.7	0.2	55	6.8	0.6
4	47	3.6	0.2	43	0.4	0.1	46	2.5	0.2
5	42	3.6	0.2	38	0.3	0.1	40	1.0	0.1
10	23	1.1	0.1	23	0.3	0.0	24	0.2	0.0
15	18	6.5	0.5	17	0.4	0.0	17	0.0	0.0

[a]Mean squared error.
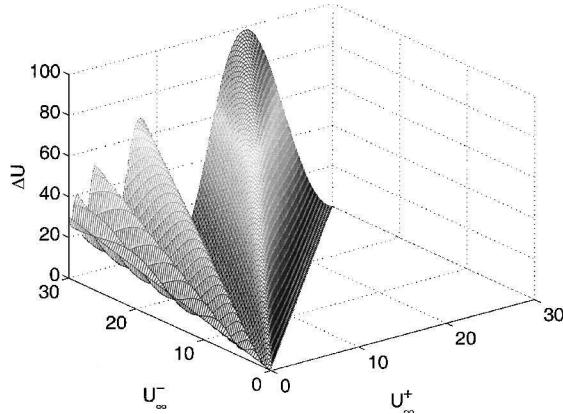
Fig. 1 ΔU as a function of U_∞^- and U_∞^+ in an AGA.
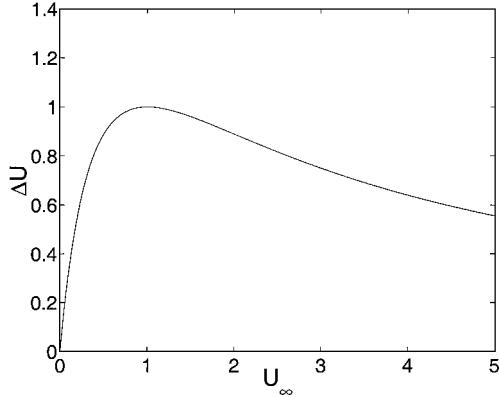
Fig. 2 ΔU as a function of U_∞ in a GA.

where ϕ is the total turn angle (gravitational and aerodynamic) given by

$$\phi = \sin^{-1}\left[\left(1 + U_\infty^-\right)^{-1}\right] + \sin^{-1}\left[\left(1 + U_\infty^+\right)^{-1}\right] + \theta \quad (4)$$

Equations (2–4) can be combined to yield an expression for ΔU explicitly in terms of U_∞^- and U_∞^+:

$$\Delta U = U_\infty^- + U_\infty^+ - 2\sqrt{U_\infty^- U_\infty^+}\cos\Big\{\sin^{-1}\left[\left(1 + U_\infty^-\right)^{-1}\right]$$
$$+ \sin^{-1}\left[\left(1 + U_\infty^+\right)^{-1}\right] + \left(\tfrac{1}{2}\right)(L/D)\,\ell n\left[\left(U_\infty^- + 1\right)\big/\left(U_\infty^+ + 1\right)\right]\Big\}$$
$$(5)$$

Figure 1 shows a graph of Eq. (5) for $L/D = 15$. Because of drag losses, $U_\infty^+ \le U_\infty^-$ in general. The special case of $U_\infty^- = U_\infty^+$ corresponds to a conventional (pure) gravity assist and is illustrated separately in Fig. 2. We note that there is a maximum ΔU for all gravity assists. For the pure gravity-assist case, we find from Eq. (5) (and see in Fig. 2) that the maximum ΔU is 1 and occurs when $U_\infty = 1$. For the AGA case, however, the maximum ΔU is unlimited and increases with increasing U_∞^-. The rippling effect in Fig. 1 is caused by the V_∞ being rotated around the planet through several

revolutions. The main lobe corresponds to the optimal turn angle to maximize ΔU (and, hence, ΔV) during the flyby. Further aerodynamic turning decreases U_∞^+ to the first valley, where V_∞^+ points in the same direction as V_∞^-. Turning beyond one revolution will again increase the ΔU, but less than before because of drag. Additional revolutions could be completed until $U_\infty^+ = 0$, at which point the spacecraft would be captured in orbit about the gravity-assist planet.

Maximizing ΔV in a Single AGA

To maximize the ΔV obtained by a single AGA, we find an analytic representation of the maximum ΔU, as a function of U_∞^-. It is not obvious from Eq. (5) that ΔU increases almost linearly, but the results shown in Fig. 1 clearly suggest this trend. We use this insight in our approximation. A different approach to this maximization is done by Elices.[16] Though Elices's approximation has the advantage of being simpler, its accuracy decreases with increasing L/D.

We start with the assumption that, for the optimal turn angle, $U_\infty^+ \approx k^2 U_\infty^-$, where k is some unknown constant, less than or equal to one. Next, we make this substitution in Eq. (3). We note that, as U_∞^- increases, the gravitational turn angles drop out of Eq. (5), and there is a quadratic/logarithmic dependence of U_∞^- on ΔU. We then solve for k in the parameter optimization

$$\lim_{U_\infty^- \to \infty} \frac{\partial}{\partial k}\Delta U = 0 \quad (6)$$

Because we are assuming U_∞^- is very large, the gravitational turn angle tends toward zero. From Eqs. (2) and (4), we see that

$$\phi = \left(\tfrac{1}{2}\right)(L/D)\,\ell n\left[\left(U_\infty^- + 1\right)\big/\left(U_\infty^+ + 1\right)\right] \approx -(L/D)\,\ell n\,k \quad (7)$$

Substituting Eq. (5) into Eq. (6) yields

$$k - \cos\phi - (L/D)\sin\phi = 0 \quad (8)$$

This transcendental equation will, in general, have several roots that correspond to the locations in Fig. 1 where a peak is reached. Because we are looking for the maximum peak solution, we pick k to be the value of the largest root. Whereas Eq. (8) can be solved numerically, an explicit form is desired. Intuitively, the optimal turn angle will be somewhat less than π. Furthermore, as $L/D \to \infty$, $k \to 1$. We use the approximations

$$\cos\phi \approx -1, \qquad \sin\phi \approx \pi - \phi = \pi + (L/D)\,\ell n\,k$$

$$\ell n\,k \approx (k - 1) + \left(\tfrac{1}{2}\right)(k - 1)^2$$

Two terms are required for the $\ell n\,k$ term to solve for k. (The linear expression is fairly inaccurate except for very high L/D ratios.)

Substituting, we obtain a quadratic expression for k:

$$k^2 + \left[\frac{2}{(L/D)^2} - 4\right]k + \left[\frac{2}{(L/D)^2} - \frac{2\pi}{L/D} + 3\right] = 0 \quad (9)$$

When the two roots in Eq. (9) are solved for, one root is always less than 1, and the other is always greater. By definition, $k \le 1$, and thus, the higher root is extraneous. Also as $L/D \to \infty$, $k \to 1$, as expected in both cases. Table 1 has a summary of the errors in these three approximations (Elices,[16] the transcendental, and the quadratic) for U_∞^- ranging from 0 to 30.

The first error listed in Table 1 is the maximum percent error in the $0 \le U_\infty \le 30$ comparison range. In all cases the largest errors occur at high values of U_∞^-. At high U_∞^- and low L/D, none of the approximations are accurate. However, the average error for all examined U_∞ is fairly small. Finally, the mean squared error (MSE) is listed for all cases. For example, suppose a spacecraft performs an AGA maneuver at Mars with an L/D of 5, an arrival V_∞ of 5 km/s, and a periapsis of 3440 km. In this case the inbound U_∞ is 2. The transcendental solution yields a maximum ΔU of 4.8. The actual maximum ΔU is 4.46. This corresponds to an 8% error, which is less than the maximum error for this case of 38% but well above the average error of 0.3%.

In the quadratic and transcendental formulations, we see that ΔU is also linearly related to U_∞^- by

$$\Delta U = U_\infty^-[1 - 2k \cos\phi + k^2] \tag{10}$$

Thus, $\Delta U/U_\infty^-$ is bounded between 1 and 4. The ΔU from an AGA will increase with increasing U_∞^-.

Not surprisingly, the transcendental expression, Eq. (8), is the most accurate (in the MSE sense) at all L/D ratios. At low L/D ratios, Elices's[16] approximation is the next most accurate. At about $L/D = 4$, the quadratic begins to do better. Because the Taylor series expansion is done about $k = 1$ (which is the case for $L/D \to \infty$), it is expected that the two methods developed here asymptotically reach zero error as L/D increases.

Optimizing for Perihelion or Aphelion in a Single AGA

Clearly AGA can potentially yield dramatic improvements in attainable ΔV over conventional gravity assists. However, unless a maximum ΔV AGA makes it easier to reach a desired destination, the attainable ΔV is useless. The turn angle that results in the maximum ΔV may not necessarily be the optimal turn angle for reaching the next body. Indeed, one of the major points of the maximum ΔV theory is to provide a benchmark for practical AGAs, that is, AGAs that actually get the spacecraft somewhere.

To this end, we examine optimizing the turn angles about the planets to maximize the spacecraft's aphelion, or to minimize its perihelion, depending on if the target body is farther from or closer to the sun. The spacecraft will then be able to reach any body in the solar system between these two bounds. The derivations that follow assume circular, coplanar planetary orbits. Figure 3 presents a vector diagram of the AGA maneuver.

$L/D = \infty$ Case

The simplest case to consider is $L/D = \infty$, where the spacecraft would not lose any V_∞ during the aerodynamic turning. This case puts a theoretical upper/lower bound on what any AGA can accomplish. No matter how waverider technology progresses, a waverider will never be able to outperform this limit.

The arrival V_∞ at the AGA planet is computed as

$$V_{\infty,2}^2 = V_2^2 + V_{pl,2}^2 - 2V_{pl,2}V_2\cos\gamma_2 = V_2^2 + V_{pl,2}^2$$

$$- 2(R_1/R_2)V_{pl,2}V_1\cos\gamma_1 = V_1^2 + V_{pl,2}^2$$

$$- 2(R_1/R_2)V_{pl,2}V_1\cos\gamma_1 + 2\mu_\odot\left(R_2^{-1} - R_1^{-1}\right) = V_{pl,1}^2$$

$$+ V_{pl,2}^2 + V_{\infty,1}^2 - 2(R_1/R_2)V_{pl,1}V_{pl,2} + 2\mu_\odot\left(R_2^{-1} - R_1^{-1}\right)$$

$$+ 2V_{\infty,1}V_{pl,1}\cos\alpha_1 - 2(R_1/R_2)V_{\infty,1}V_{pl,2}\cos\alpha_1 \tag{11}$$
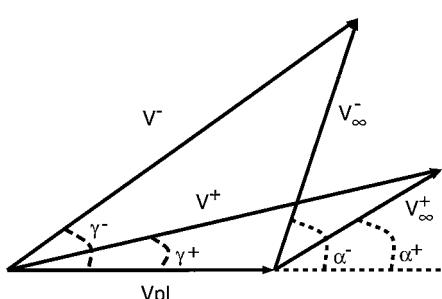

Fig. 3   AGA vector diagram.

Now that we have an expression for the arrival V_∞ at the AGA planet in terms of departure conditions at Earth, we can find the optimum α_1 to maximize $V_{\infty,2}$. The first and second derivative rules tell us that $\alpha_1 = 0$ deg if $R_2 > R_1$, or $\alpha_1 = 180$ deg, if $R_2 < R_1$. In the $R_2 > R_1$ case, we maximize aphelion, and we minimize perihelion in the $R_1 < R_2$ case.

With an L/D of ∞, a spacecraft can turn any desired turn angle without losing V_∞. The Hohmann transfer shows that a tangential ΔV is optimum for maximizing aphelion or minimizing perihelion. Thus, the optimum turn angle in this case makes the $\boldsymbol{V}_\infty$ parallel to the planet's velocity vector (this is not true for the finite L/D case because rotating the $\boldsymbol{V}_\infty$ also decreases its magnitude). For a tangential departure, maximizing heliocentric velocity is equivalent to maximizing aphelion (and similarly, minimizing heliocentric velocity is equivalent to minimizing perihelion); we know that $V_2^+ = V_{pl,2} \pm V_{\infty,2}$.

Thus, maximum aphelion or minimum perihelion can be computed as

$$R_{a,p} = R_2[U_2/(2 - U_2)] \tag{12}$$

where, in this sense, $U_2 = V_2^2 R_2/\mu_\odot$.

Equation (12) is derived assuming the spacecraft departs Earth and executes an AGA at the next planet in its path sequence. Furthermore, because [as shown in Eq. (11)] tangential Earth departures are optimal in this sense, and because tangential AGA planet departures are optimal, we can patch several of these trajectories together to get the optimal multibody trajectory. The optimal multibody trajectory departs each body tangentially as to maximize the arrival V_∞ at the next body. When the spacecraft arrives at the next body, it turns so it leaves tangentially to go on to the next planet.

Finite L/D Case

Of course, infinite L/D ratios are impossible. A parameter optimization problem can be set up for the finite L/D case similar to the infinite L/D case. However, V_∞^+ is now a function of V_∞^- and θ. Launching tangentially from Earth is also not necessarily optimal. For a single-body AGA, maximizing aphelion or minimizing perihelion can be formulated as a two-dimensional parameter optimization problem for a given L/D and launch V_∞. An analytic solution appears intractable, and so a numerical solution is calculated. The results are presented in Figs. 4 and 5.

Figure 4 shows the maximum aphelion and minimum perihelion possible with a single AGA at Venus for several different L/D ratios. The Venus gravity assist (VGA) and Venus AGA (VAGA) contours start from a launch V_∞ of 2.5 km/s, which corresponds to the Hohmann transfer. We note that, at this launch V_∞, it is impossible to increase aphelion, because the spacecraft arrives at Venus with its $\boldsymbol{V}_\infty$ aligned with the velocity vector of Venus, that is, $\alpha = 0$. However, it is still possible to decrease perihelion. The more turning that can be accomplished, that is, the higher the L/D ratio, the lower the perihelion can be. The ability to decrease perihelion for the Hohmann transfer is the cause for the apparent discontinuity in Fig. 4; the Hohmann transfer provides a perihelion at Venus, but we can immediately get additional bending to decrease perihelion even further.

As the launch V_∞ increases, so does the arrival V_∞ at Venus. Furthermore, α also increases. Aphelion can be increased by rotating the $\boldsymbol{V}_\infty$ back toward $\alpha = 0$ deg. For launch V_∞ less than 3.2 km/s, a pure VGA is able to achieve maximum turning (without overturning the $\boldsymbol{V}_\infty$). Thus, an AGA is not needed, but for launch V_∞ higher than 3.2 km/s, a VAGA more effectively increases aphelion. We see in Fig. 4 that, even for a launch V_∞ as high as 15 km/s, a pure VGA cannot reach Jupiter. For a high launch V_∞, there is a correspondingly high α at the VGA. However, with high arrival V_∞ at Venus, the maximum turn angle is insufficient to rotate the $\boldsymbol{V}_\infty$ enough to increase the spacecraft's heliocentric velocity (and therefore, its energy). A VAGA does not suffer this disadvantage because the $\boldsymbol{V}_\infty$ can be rotated to an arbitrary direction. The aerodynamic portion of a turn is responsible for most of the turning at high arrival V_∞, unlike low arrival V_∞ where gravity dominates.

Because Figs. 4 and 5 represent aphelion and perihelion distances, the points where a contour intersects a planet imply the spacecraft
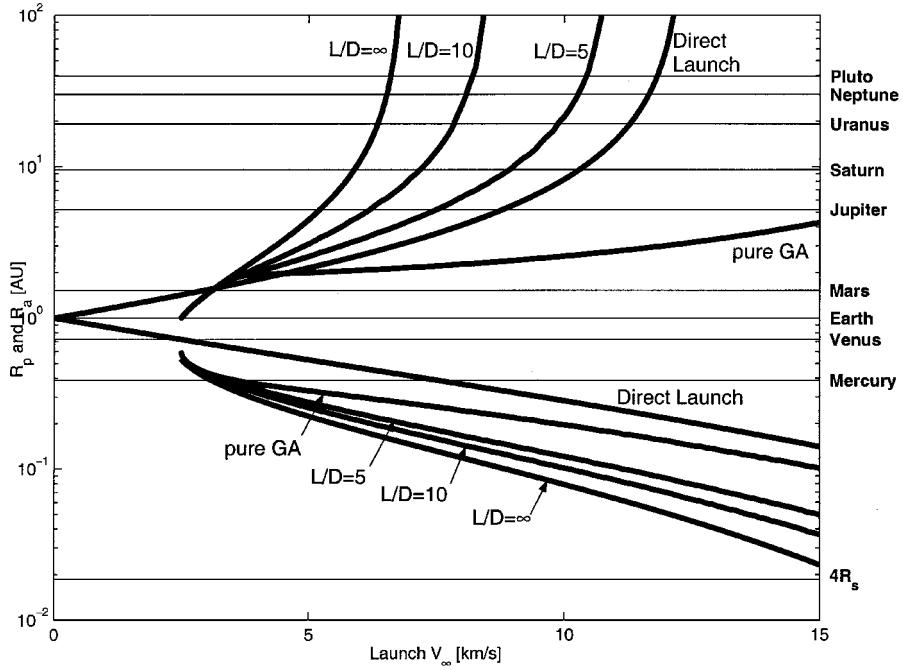
Fig. 4   Maximizing aphelion or minimizing perihelion using a single VAGA.
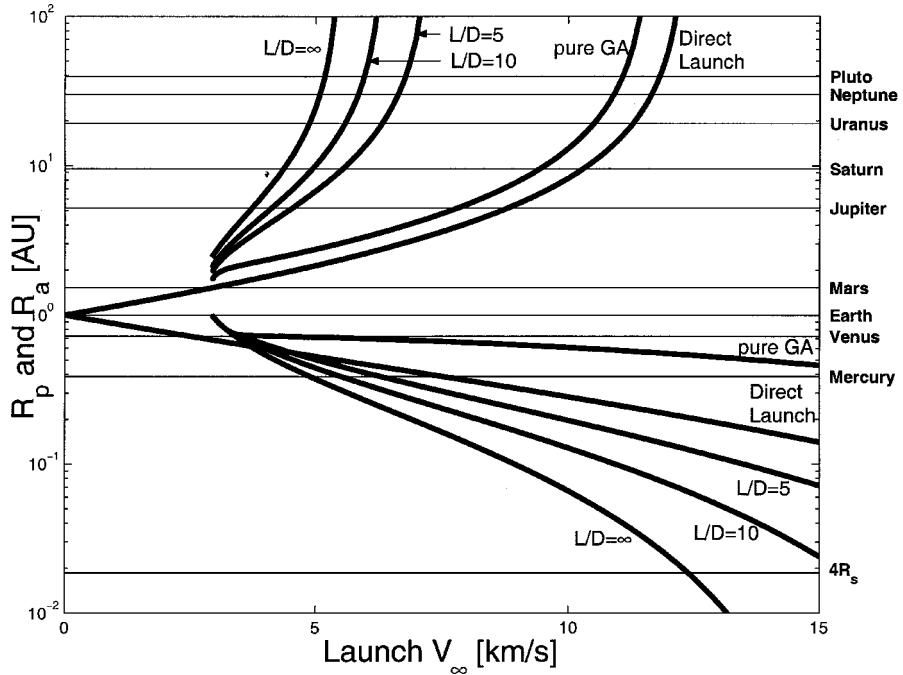
Fig. 5   Maximizing aphelion or minimizing perihelion using a single MAGA.

arrives tangentially. Also, the $L/D = \infty$ case must always depart Venus tangentially because this provides the extremal heliocentric velocity. Therefore, points where the $L/D = \infty$ contour intersect a planet are all identical to Hohmann transfers from Venus to that planet and may have fairly lengthy TOFs. For all finite L/D contours, the departure α will be somewhat larger. Thus, Venus will not be at perihelion (if traveling upwell) or aphelion (if traveling downwell). Although the TOFs will be shorter, they are not much more so if traveling to the outer planets and come at the cost of increased launch V_∞.

In many ways, Mars behaves inversely to Venus. Figure 5 shows the Mars gravity assist (MGA) and the Mars AGA (MAGA). At the Hohmann launch V_∞, it is impossible to decrease perihelion; however, aphelion can be increased. Furthermore, the MGA is capable

of full turning for launch V_∞ less than 3.2 km/s. The arc where gravity alone is sufficient is smaller than that of Venus because Mars has lower gravity. Because of this lower gravity, the MGA can barely rotate the V_∞ at higher arrival V_∞. However, the MAGA is still able to because the departure direction is unconstrained. The large gap in increasing aphelion between the pure MGA case and the $L/D = 5$ case occurs because of the MAGA's ability to have an arbitrary departure angle. A single MAGA allows a spacecraft to reach Jupiter instead of requiring the traditional 2 or 3 flybys of other planets. At the launch V_∞ for an MGA to reach Jupiter, a MAGA is easily capable of escaping the solar system.

A MAGA is also more capable of decreasing perihelion at higher launch V_∞ than a VAGA. Decreasing perihelion is equivalent to reducing heliocentric velocity during a flyby. For any gravity-assist

body, the goal is to rotate the spacecraft's V_∞ to be parallel and opposite in direction to the planet's velocity vector. Because the departure direction is arbitrary for an AGA, and the heliocentric velocity of Mars is much smaller than that of Venus, a MAGA is able to reduce perihelion more than a VAGA can, for the same flyby V_∞.

When there are more than one or two AGA planets to consider, this graphical method becomes cumbersome and does not provide much insight. An alternate method is developed instead.

Tisserand Analysis

A graphical tour design method based on Tisserand's criterion (and referred to as Tisserand graphs) was developed to aid in searching for paths for the Europa Orbiter mission (see Refs. 17 and 18). Two orbital elements completely describe the shape of a spacecraft's orbit. If we assume that the planets are in circular, coplanar orbits around the sun, then the arrival geometry for the spacecraft at a given planet is also known. Plotting contours of a third parameter from the first two results in a Tisserand graph. For the Europa Orbiter case, period and periapsis radius with respect to Jupiter were selected as the independent quantities. We use specific orbital energy instead of period because many conic arcs to the outer planets are hyperbolic with respect to the sun. Because these two quantities provide the orbit shape, the flyby conditions are known when that orbit crosses a given body's path. In particular, the arrival V_∞ is known for a given E, R_p, and flyby planet. From Fig. 3 we have that

$$V_\infty^2 = V_{pl}^2 + V^2 - 2V_{pl}V\cos\gamma = V_{pl}^2 + 2E + 2\mu_\odot/R - 2V_{pl}V\cos\gamma$$

$$= V_{pl}^2 + 2E + 2\mu_\odot/R - 2(R_p/R)V_{pl}\sqrt{2E + 2\mu_\odot/R_p}$$

$$= 2E + 3\mu_\odot/R - 2(R_p/R)\sqrt{2(\mu_\odot/R)(E + \mu_\odot/R_p)} \quad (13)$$

In pure gravity assists, the pre- and post-V_∞ are the same, but the orbits (which are points on a Tisserand graph) are different. A gravity assist is graphically depicted as following constant V_∞ contours on a Tisserand graph, as shown in Fig. 6. The distance on a contour that can be traversed by a single flyby depends (in part) on the radius of the flyby body, that is, when a flyby approaches the surface, further turning is not possible. The tick marks (dots) on the plot denote contour distance at maximum turning. Figure 6 shows that Mars is not a very effective gravity-assist body because its tick marks are very close together. On the other hand, Jupiter's tick marks are spread out, and therefore, Jupiter is much more capable of altering a spacecraft's orbit.

An AGA further spreads out the tick marks. Let us consider the hypothetical $L/D = \infty$ case where the V_∞ can be turned to any desired direction. This case corresponds to moving the tick marks to the endpoints of the contours. Finite L/D values complicate matters because the V_∞ does not remain constant. As the aerodynamic turn angle increases, the V_∞^+ decreases. However, this loss may
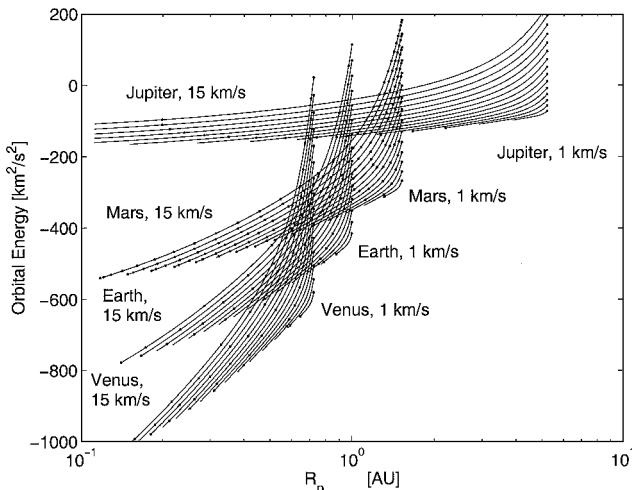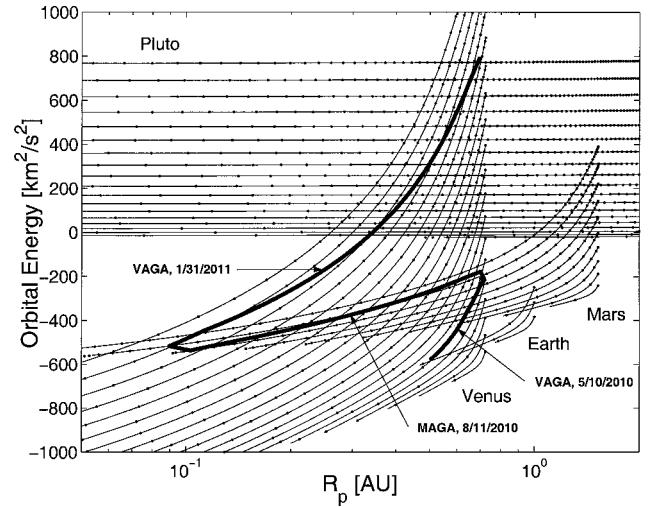
Fig. 7   Tisserand graph of an EVMVP trajectory using AGA.
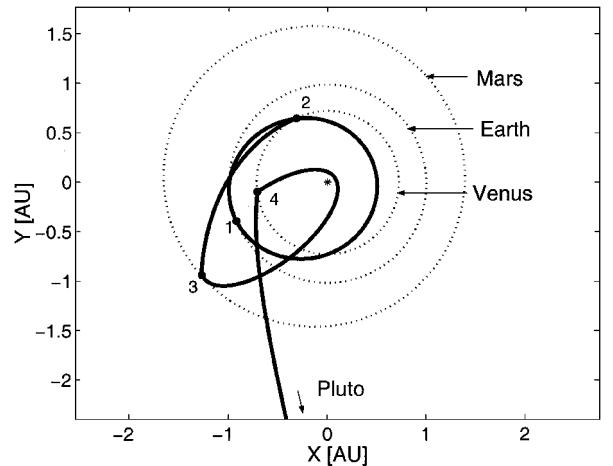
Fig. 8   Polar view of an EVMVP trajectory using AGA.

be worthwhile because the tick mark constraint is no longer valid. With these facts combined, a sample trajectory to Pluto is shown in Fig. 7.

In Fig. 6, the V_∞ contours start at the lower-right corner at $V_\infty = 1$ km/s for each of the planets. The spacing between contours is also 1 km/s. In Fig. 7, the contour spacings are at 2 km/s for clarity. This Tisserand graph depicts a trajectory found in STOUR that launches from Earth on 13 April 2009 with a V_∞ of 6.0 km/s and travels to Pluto via a VAGA, a MAGA, and another VAGA. For comparison, a polar view of this same trajectory is shown in Fig. 8. From Fig. 7, we see that the launch V_∞ contour intersects several Venusian V_∞ contours, meaning that the spacecraft can coast from Earth to Venus. We use one phasing orbit to reach Venus, that is, a type IV trajectory to Venus. The phasing orbit is not apparent on the Tisserand graph because the graph does not distinguish between single- and multiple-revolution transfers. The spacecraft arrives at Venus on 10 May 2010 with an arrival V_∞ of 12.3 km/s and performs a VAGA to reach Mars. The VAGA is graphically depicted by tracing a Venusian contour upward to reach the Mars contours. If a VGA were done instead, the spacecraft would be limited in its turning (it can cross only one tick mark). With an AGA, the spacecraft can get some free gravitational turning, but the rest of the turning will result in loss of V_∞. In this case, the spacecraft leaves Venus with a V_∞ of only 10.7 km/s. This turning allows the spacecraft to arrive at Mars with a V_∞ of 18.9 km/s on 11 August 2010. The spacecraft performs another AGA, which lowers its Mars V_∞ to 16.0 km/s, while also drastically pumping down its perihelion to 0.086 astronomical units (AU) (or about 18 solar radii). This is shown on the Tisserand graph by following a Mars contour to the left. The spacecraft coasts to Venus, arriving 31 January 2011,

Fig. 6   Tisserand graph.

where a final VAGA pumps up the heliocentric energy to a hyperbolic orbit. From Venus, the spacecraft arrives at Pluto on 5 October 2014.

Viterbi Algorithm

The Tisserand graph provides a valuable tool for examining gravity assist (GA) or AGA trajectories. However, the decaying V_∞ in the AGA maneuver complicates the interpretation of the graph. For this reason, a computer program was written to search through the Tisserand graph's contours to find the shortest TOF trajectory from Earth to every other planet. The program calculates both GA and AGA cases for any number of flyby bodies. However, because of the circular, coplanar assumption, and the lack of phasing (timing) information, any hypothetical trajectory still needs to be verified by other means.

We discretize the Tisserand graph into a collection of nodes. The orbital state vector after a flyby is then mapped to the nearest node. Thus, the finer the discretization, the smaller the error in the algorithm. There are up to four possible coast arcs from one planet to another for each point in the Tisserand graph[17] (only two arcs are possible for hyperbolic trajectories). All possible arcs are considered, keeping the direction of the trajectory consistent for each arc. A large number of trajectories (billions or more) must be considered. To drastically cut back on search time, while ensuring each optimal trajectory is found, we employ the Viterbi algorithm.[19] This algorithm finds the minimum-TOF path between any desired initial and final condition in the minimal number of comparisons. The results that follow are based on the Viterbi algorithm and the minimum-TOF path, which ignores phasing. The predicted AGA paths must be verified by solving the Lambert problem, which is addressed in the next section.

The AGA results for Mars and Venus are unremarkable because no GAs are needed to reach them. The optimal trajectory from Earth to Mercury involves at least one flyby at Venus. For launch V_∞ higher than 4 km/s, the TOF savings with AGA is minimal. A summary of results for trajectories to Mercury (Y) is presented in Table 2.

For a launch V_∞ of 3 km/s, a single VAGA is insufficient to reach Mercury; furthermore, it is impossible to reach Mercury with only two flybys. The fastest potential three-flyby trajectory to Mercury uses a Venus–Earth–Venus combination of AGAs for a TOF of 0.79 years. Additional flybys beyond the third increases the TOF and, thus, are unnecessary. For launch V_∞ of ≥ 4 km/s, a single

VAGA is sufficient to reach Mercury. The TOF cannot be improved with additional flybys.

The biggest advantage of AGA is in missions to the outer planets. A summary of results is shown in Table 3. Dashes mean that no such trajectory is possible (due to insufficient launch energy). For example, no trajectory to Saturn using only one flyby body exists for a launch V_∞ of 5 km/s, that is, the V_∞^- must be high enough to make AGA effective.

Because this analysis does not take into account phasing (however, it does allow for resonant flybys), the existence of a trajectory that returns to a given planet is not guaranteed. In general, the greater the number of times a given planet is used (excluding resonant flybys), the less likely such a trajectory will, in fact, exist at all.

Our algorithm allows for an AGA at all planets except Mercury and Pluto (which do not have appreciable atmospheres). Interestingly enough, the time-optimal trajectories rely most heavily on Venus and Mars and only occasionally use Earth. For many of the cases, the optimal trajectory is an alternating series of Venus, Earth, and Mars AGAs until the destination planet is reached. Because the inner planets' orbits have such low semimajor axes compared to the outer planets, using them exclusively (since we can get arbitrary bending at them) is better than hoping all of the outer planets line up right. For example, the best trajectory to Pluto with a launch V_∞ of 6 km/s uses a Venus–Mars–Venus–Mars series of AGAs, as opposed to using Jupiter, Saturn, Uranus, or Neptune (even though AGAs are also allowed at these planets). Whereas Jupiter is a powerful GA planet, it is too far away to compete effectively with the inner planets when AGAs are used (except when substantial inclination changes are needed). Another factor evident from examining Fig. 6 is that, if Jupiter is used to pump up a spacecraft's energy, then its semimajor axis is greatly increased. A Jupiter AGA of this fashion unacceptably lengthens the size and TOF of the conic arc to the next planet, and thus, Jupiter does not appear in the fastest trajectories found in the search. Thus, we do not have to depend on phasing with Jupiter to get to the outer planets, only on the phasing of Venus, Earth, and Mars.

Considering trajectories to Pluto for a launch V_∞ of 6.0 km/s, we see that adding a third flyby lowers the TOF to 5.7 years. This trajectory is, in fact, the Earth–Venus–Mars–Venus–Pluto (EVMVP) discussed earlier. However, the actual TOF may be much shorter because Pluto is currently about 30 AU away from the sun, whereas our algorithm assumes a constant semimajor axis of approximately 40 AU. A more fair comparison would be to Neptune, which has a lower bound of 4.45 years using the Venus–Mars–Venus (VMV) sequence of AGAs at a launch V_∞ of 6.0 km/s.

The EVMVP trajectory was examined in more detail using STOUR for a 40-year launch window (2000–2040) and launch V_∞ ranging from 4.0 to 6.0 km/s. The results are shown in Fig. 9. The trajectory is indicated by the "path" label, where the number n corresponds to the nth planet from the sun. The "lift/drag" field gives the L/D ratios used at each flyby planet. In this case, an L/D of 7 was used during the Venus and Mars encounters. Finally, the plot itself comprises several letters. Each of these represents a trajectory

Table 2   Fastest potential AGA trajectories to Mercury with $L/D = 7$ (ignoring phasing)

Launch V_∞, km/s	Path	TOF, years
3	EVEVY	0.79
4	EVY	0.37
5	EVY	0.30
6	EVY	0.27

Table 3   Fastest potential AGA trajectories to the outer planets with $L/D = 7$ (ignoring phasing)

V_∞, km/s	Jupiter (J)		Saturn (S)		Uranus (U)		Neptune (N)		Pluto	
	Path	TOF, years	Path	TOF, years	Path	TOF, years	Path	TOF, years	Path	TOF, years
3	EVEMJ	1.99	EVEMS	3.53	EVEMU	8.21	EVEMN	15.33	EVEMP	23.08
3	EVEVMJ	1.64	EVEVMS	2.43	EVEVMU	4.24	EVEVMN	6.35	EVEVMP	8.21
3	EVEVEMJ	1.56	EVEVMVS	2.20	EVEVMVU	3.46	EVEVMVN	4.91	EVEVMVP	6.18
4	EVMJ	2.20	EVMS	5.61	——		——		——	
4	EVEMJ	1.43	EVEMS	2.44	EVMVU	4.71	EVMVN	7.21	EVMVP	9.44
4	EVEMVJ	1.36	EVEMVS	1.92	EVEMVU	3.20	EVEMVN	4.65	EVEMVP	5.93
4	EVEMVEJ	1.32	EVEMVES	1.87	EVEMVEU	3.14	EVEMVEN	4.58	EVEMVEP	5.85
5	EMJ	2.46	——		——		——		——	
5	EVMJ	1.46	EVMS	2.61	EVMU	5.52	EVMN	9.14	EVMP	12.45
5	EVEMJ	1.24	EVMVS	2.08	EVMVU	3.53	EVMVN	5.18	EVMVP	6.63
5	EVEMVJ	1.23	EVEMVS	1.78	EVEMVU	3.04	EVEMVN	4.49	EVEMVP	5.76
6	EMJ	1.68	EMS	3.64	EMU	14.16	——		——	
6	EVMJ	1.27	EVMS	2.21	EMVU	4.41	EMVN	6.96	EMVP	9.23
6	EVEMJ	1.11	EVMVS	1.74	EVMVU	3.00	EVMVN	4.45	EVMVP	5.72

PATH: 3 2 4 2 9   LIFT/DRAG: 0.0 7.0 7.0 7.0 0.0
VINF(KM/S): 4.00 4.50 5.00 5.50 6.00
SEARCH EVENT NO.: 5 ALTMIN = 0 KM SEARCH MIN. ALT.: 0 KM

LAUNCH DATES SEARCHED: 00/ 1/ 1 TO 40/ 1/ 1 BY 15.0 DAYS
TFMAX = 2850.0 DAYS (7.8 YRS)
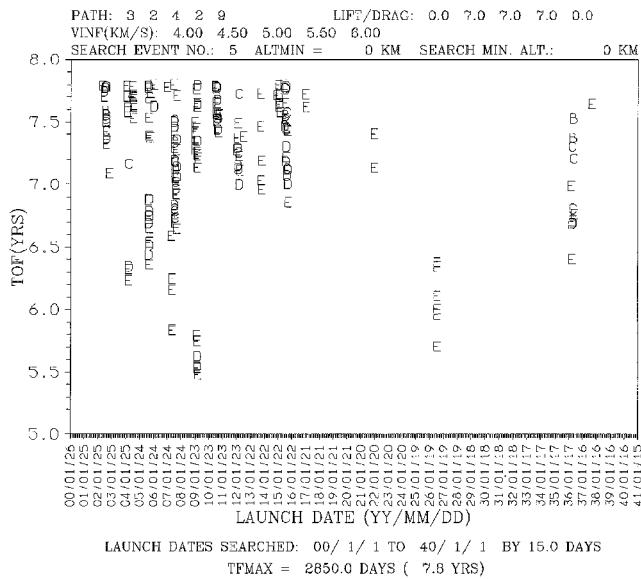
Fig. 9 VMV AGA trajectories to Pluto.

Fig. 10 Shortest TOF trajectories to Pluto with a given maximum g-load constraint.

Fig. 11 Shortest TOF trajectories to Mercury with a given maximum g-load constraint.

with the indicated launch date and TOF. The letter itself is an index for the launch V_∞ values that are searched. In this case, an A represents a launch V_∞ of 4.00 km/s; a B represents a launch V_∞ of 4.50 km/s, and so on.

With the given conditions, the fastest trajectory to Pluto has a launch V_∞ of 6.0 km/s and takes only 5.5 years. If we use a launch V_∞ of only 5.5 km/s instead, the spacecraft gets there only slightly later. Other trajectories with slightly longer TOFs are possible every few years. These extremely low TOF trajectories to Pluto begin to disappear as Pluto moves farther away (at later launch windows). Even with a lower L/D ratio of 5, the VMV trajectory still yields short TOFs, somewhat less than a year longer than the $L/D = 7$ case. Work by Sims et al.[9] indicates that lower L/D ratios will yield trajectories to the outer planets that are 1–2 years longer than the infinite L/D case. Earlier work by Bonfiglio[10] yielded AGA trajectories that either took 5 years longer for the same launch energy or took 4 years longer for an increased launch energy of 7 km/s, compared to our fastest AGA trajectory to Pluto (5.5 years for a launch V_∞ of 6.0 km/s). Clearly, the Tisserand graphical method is a powerful tool in identifying short TOF, low launch energy trajectories.

Patched-Conic Results

The Tisserand graphs are ultimately just a tool to help find good paths. Once a path has been identified, a patched-conic solver can search for actual trajectories over a spread of launch conditions. The paths from Tables 2 and 3 were used to search for both pure GA and AGA trajectories to Mercury and Pluto over a 40-year launch window.

For missions to Pluto, TOF and launch V_∞ will be of great concern. However, for practical reasons, we do not want to subject the spacecraft to excessive g-loading. Figure 10 shows the best TOF to Pluto possible through the year 2040 for a launch V_∞ of 6.0 km/s and a given maximum g-load constraint. Aerodynamic heating is also of great concern, but fully addressing heating is beyond the scope of this paper. However, g-loading scales with V^2, and heating scales with V^3 (Refs. 14 and 20). Thus, the relative ordering of results for heating should be the same as for g loading. If TOF were not a consideration, the trajectory that offers the smallest maximum g loading is Earth–Venus–Earth–Pluto (EVEP). However, if g loads of up to 7 g are tolerable, the Earth–Mars–Earth–Pluto (EMEP) is the trajectory that is capable of getting to Pluto fastest. If the g-load constraint is over 8 g, the EVMVP trajectory is the best. The performance of the EVMVP begins to asymptotically approach five years beyond the 13-g constraint (or equivalently, under 5.5 years TOF). Pushing the AGA beyond that limit yields quickly diminishing returns and would not be very useful. The other five trajectories shown in Fig. 10 never yield the fastest trajectory for any given
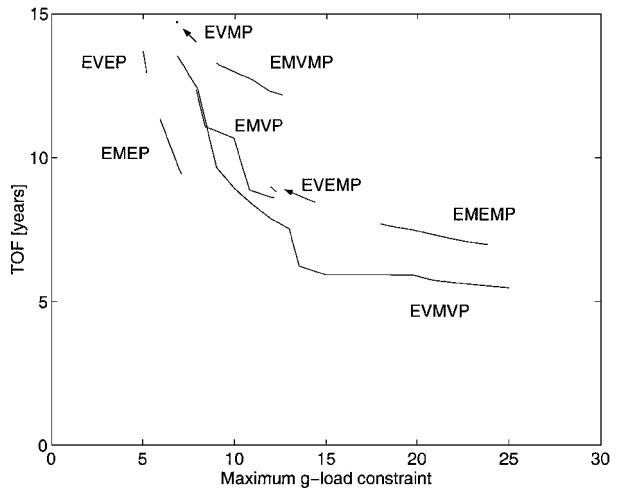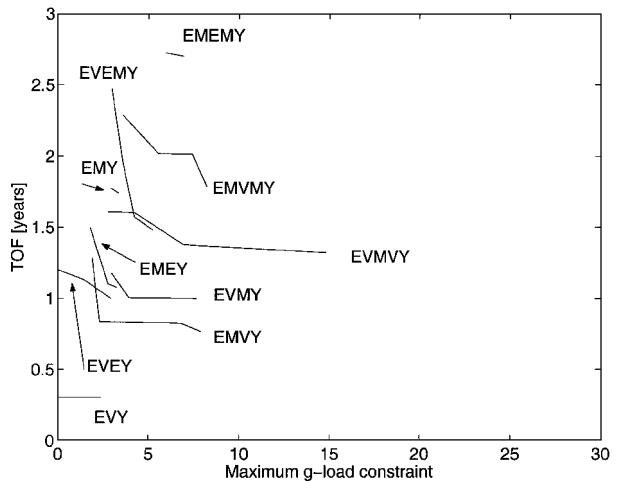
g-load constraint and, thus, would also never be used. We note that the three optimal trajectories have a commonality: they each use exactly two distinct planets in an alternating fashion [such as VMV or Venus–Earth–Venus (VEV)].

A similar graph can be made for missions to Mercury, as seen in Fig. 11. In this case, it is possible to get to Mercury with a launch V_∞ of 5.0 km/s using a pure GA trajectory [an Earth–Venus–Mercury (EVY), where we use the last letter of Mercury to distinguish it from Mars]. Furthermore, using an AGA does not shorten the TOF below that of the EVY. Thus, for a launch V_∞ of 5.0 km/s, a pure GA at Venus provides the time-optimal trajectory to Mercury.

Flight times to Mercury are relatively short, but an AGA provides other advantages. Figure 12 shows the trajectories to Mercury now optimized for lowest arrival V_∞. The pure GA EVY has an arrival V_∞ of 8.4 km/s. Once we allow AGA trajectories, the optimum arrival V_∞ is lowered to 5.9 km/s for only 2.5 g. Thus the AGA permits a Hohmann transfer from Venus to Mercury and only requires a single Venus flyby.

Discussion

Earlier we found the optimal atmospheric turn angle to maximize ΔV, but we also know that this ΔV may not be pointing in the right direction to get to the next planet. We can find the necessary conditions for a maximum ΔV AGA to accomplish this by inspecting the Tisserand graph (Fig. 6).

If an AGA begins near one of the endpoints of a V_∞ contour (far lower left or far upper right), then a maximum ΔV AGA would drive the spacecraft toward the other endpoint (but at a lower contour because some V_∞ is lost). However, a maximum ΔV AGA maneuver that begins near the middle of a V_∞ contour would follow
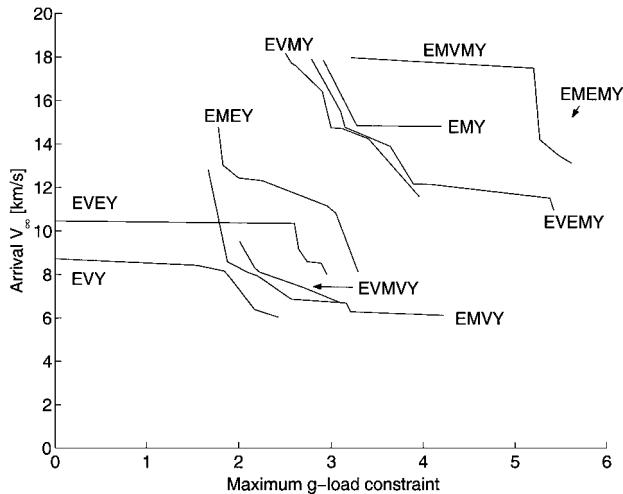
Fig. 12   Lowest arrival V_∞ trajectories to Mercury with a given maximum g-load constraint.

the contour in one direction and then backtrack (overturn), only to end up near where the maneuver began. Overturning results in a large change in the spacecraft's true anomaly but little change in the shape of the orbit itself. A smaller turn angle gives an equivalent turn, but with less loss of V_∞. Thus, the most efficient ΔV possible with an AGA are the ones that arrive and depart the flyby body nearly tangentially. The limiting case occurs when $L/D = \infty$, where the spacecraft arrives and departs exactly tangentially. The near-tangential arrival/departure condition is met in the earlier discussed EVMVP trajectory of Fig. 7. As seen in Fig. 7, all three AGAs are located near the endpoint of a V_∞ contour. However, simply arriving or departing a contour near an endpoint is insufficient for maximizing ΔV for a given L/D. Because the optimal turn angle is a function of L/D, higher L/D ratios permit greater travel along the V_∞ contours. For $L/D = 7$, Eqs. (7) and (9) yield $\phi \approx 174$ deg, so that the AGA maneuver travels through about 97% of a V_∞ contour. Clearly, the AGAs in Fig. 7 are not ΔV maximum because the AGAs begin in the middle of a contour. However, due to the geometry of the contours, maximum ΔV AGAs are not possible for the EVMVP case at higher L/D ratios, that is, an AGA is capable of providing a ΔV in excess of what is optimal for reaching the next body. Therefore, a lower L/D ratio exists such that a maximum ΔV AGA is possible and optimal for a specific maneuver. The AGAs in Fig. 7 do turn the maximum amount without overturning. Moreover, even when a maximum ΔV trajectory exists, it may not be time optimal. From Fig. 7, we see that an Earth–Venus–Mars–Pluto (EVMP) is possible using a maximum ΔV AGA with a Mars V_∞^- of 10 km/s. However, from Table 3, we know that the EVMVP is faster than the EVMP. Even with a series of AGAs that do not use 100% of the possible ΔV, the trajectory can be faster than any comparable pure GA trajectory.

Conclusions

An AGA can potentially yield much higher ΔV than a pure GA, and the Tisserand graph shows when it is possible. The real power of AGA is apparent when multiple AGA flybys are used, especially when one body acts as a V_∞-leveraging maneuver for another [such as a VMV or Mars–Venus–Mars (MVM)]. These trajectories allow for extremely fast missions with low launch energies. Unfortunately, using multiple AGA encounters has some disadvantages. The high ΔV involved with AGA is what enables the low launch V_∞, short TOF trajectories. This directly translates to high approach V_∞ and high acceleration and heating loads. The heating will ablate the waverider and degrade its aerodynamic properties, making subsequent AGA passes more difficult.

As seen from the Tisserand analysis, the Earth is not used as often for AGA because it has only a moderate effect on the orbit shape. On the other hand, Mars and Venus can be quite effective. Venus is typically most useful in changing the orbital energy of a spacecraft, whereas Mars is typically most useful in changing a spacecraft's

perihelion. Earth can do both, but neither quite as well as Mars or Venus. The outer planets are too far away to be useful as AGA bodies.

AGA provides three significant advantages. First, trajectories do not have to rely on phasing of the outer planets (aside from the target) but only on Venus, Earth, and Mars. Second, TOFs are small. Because the initial phase of an AGA trajectory will usually rely only on Venus and Mars, the time required to build up the spacecraft's orbital energy is kept to a minimum. Finally, fast trajectories to all planets exist using low launch energy.

The AGA technique provides exciting new trajectories to difficult targets in the solar system. For example, Pluto can be reached in only 5.5 years using a VMV AGA, for a L/D of 7, with a launch V_∞ of 6.0 km/s. The trajectories presented here supply compelling reasons to develop high L/D hypersonic vehicles (such as the waverider). The development of AGA technology will enable deep space exploration at low launch energy and for short flight time.

References

[1]Sims, J., Staugler, A., and Longuski, J., "Trajectory Options to Pluto via Gravity Assists from Venus, Mars, and Jupiter," *Journal of Spacecraft and Rockets*, Vol. 34, No. 3, 1997, pp. 347–353.

[2]Petropoulos, A., Longuski, J., and Vinh, N., "Shape-Based Analytic Representations of Low-Thrust Trajectories for Gravity-Assist Applications," American Astronomical Society, AAS Paper 99-337, Aug. 1999.

[3]Nonweiler, T., "Aerodynamic Problems of Manned Space Vehicles," *Journal of the Royal Aeronautics Society*, Vol. 63, Sept. 1959, pp. 521–528.

[4]Lewis, M., and McRonald, A., "Design of Hypersonic Waveriders for Aeroassisted Interpanetary Trajectories," *Journal of Spacecraft and Rockets*, Vol. 29, No. 5, 1992, pp. 653–660.

[5]Starkey, R., and Lewis, M., "Simple Analytical Model for Parametric Studies of Hypersonic Waveriders," *Journal of Spacecraft and Rockets*, Vol. 36, No. 4, 1999, pp. 516–523.

[6]Starkey, R., and Lewis, M., "Analytical Off-Design Lift-to-Drag-Ratio Analysis for Hypersonic Waveriders," *Journal of Spacecraft and Rockets*, Vol. 37, No. 5, 2000, pp. 684–691.

[7]Randolph, J., and McRonald, A., "Solar System 'Fast Mission' Trajectories Using Aerogravity Assist," *Journal of Spacecraft and Rockets*, Vol. 29, No. 2, 1992, pp. 223–232.

[8]McRonald, A., and Randolph, J., "Hypersonic Maneuvering for Planetary Gravity Assist," *Journal of Spacecraft and Rockets*, Vol. 29, No. 2, 1992, pp. 216–222.

[9]Sims, J., Longuski, J., and Patel, M., "Aerogravity-Assist Trajectories to the Outer Planets and the Effect of Drag," *Journal of Spacecraft and Rockets*, Vol. 37, No. 1, 2000, pp. 49–55.

[10]Bonfiglio, E., "Automated Design of Gravity-Assist and Aerogravity-Assist Trajectories," M.S. Thesis, School of Aeronautics and Astronautics, Purdue Univ., West Lafayette, IN, Aug. 1999.

[11]Rinderle, E., "Galileo User's Guide, Mission Design System, Satellite Tour Analysis and Design Subsystem," Jet Propulsion Lab., JPL Pub. D-263, California Inst. of Technology, Pasadena, CA, July 1986.

[12]Lohar, F., Mateescu, D., and Misra, A., "Optimal Atmospheric Trajectory for Aerogravity Assist," *Acta Astronautica*, Vol. 32, No. 2, 1994, pp. 89–96.

[13]Lohar, F., Misra, A., and Mateescu, D., "Optimal Aero-Gravity Assist with Heliocentric Plane Change," *Acta Astronautica*, Vol. 38, No. 4–8, 1996, pp. 445–456.

[14]Lohar, F., Misra, A., and Mateescu, D., "Optimal Atmospheric Trajectory for Aerogravity Assist with Heat Constraint," *Journal of Guidance, Control, and Dynamics*, Vol. 18, No. 4, 1995, pp. 723–730.

[15]Anderson, J., Lewis, M., Kothari, A., and Corda, S., "Hypersonic Waveriders for Planetary Atmospheres," *Journal of Spacecraft and Rockets*, Vol. 28, No. 4, 1991, pp. 401–410.

[16]Elices, T., "Maximum ΔV in the Aerogravity Assist Maneuver," *Journal of Spacecraft and Rockets*, Vol. 32, No. 5, 1995, pp. 921, 922.

[17]Strange, N. J., and Longuski, J. M., "Graphical Method for Gravity Assist Trajectory Design," *Journal of Spacecraft and Rockets*, Vol. 39, No. 1, 2002, pp. 9–16; also AIAA Paper 2000-4030, Aug. 2000.

[18]Heaton, A. F., Strange, N. J., Longuski, J. M., and Bonfiglio, E. P., "Automated Design of the Europa Orbiter Tour," *Journal of Spacecraft and Rockets*, Vol. 39, No. 1, 2002, pp. 17–22; also AIAA Paper 2000-4034, Aug. 2000.

[19]Viterbi, A., "Error Bounds for Convolutional Codes and an Asymptotically Optimal Decoding Algorithm," *IEEE Transactions on Information Theory*, Vol. IT-13, April 1967, pp. 260–269.

[20]Vinh, N., Busemann, A., and Culp, R., *Hypersonic and Planetary Entry Flight Mechanics*, Univ. of Michigan Press, Ann Arbor, MI, 1980, Chaps. 2 and 9.